

Metal-insulator transition of spinless fermions coupled to dispersive optical bosons

Florian Lange^{1,*} and Holger Fehske^{1,2,+}

¹Friedrich-Alexander-Universität Erlangen-Nürnberg (FAU), Erlangen National High Performance Computing Center (NHR@FAU), 91058 Erlangen, Germany

²Institute of Physics, University of Greifswald, 17489 Greifswald, Germany

*florian.lange@fau.de

+holger.fehske@fau.de

ABSTRACT

Including the previously ignored dispersion of phonons we revisit the metal-insulator transition problem in one-dimensional electron-phonon systems on the basis of a modified spinless fermion Holstein model. Using matrix-product-state techniques we determine the global ground-state phase diagram in the thermodynamic limit for the one-dimensional band case, and show that in particular the curvature of the bare phonon band has a significant effect, not only on the transport properties characterized by the conductance and the Luttinger liquid parameter, but also on the phase space structure of the model as a whole. While a downward curved (convex) dispersion of the phonons only shifts the Tomonaga-Luttinger-liquid to charge-density-wave quantum phase transition towards stronger EP coupling, an upward curved (concave) phonon band leads to a new phase-separated state which, in the case of strong dispersion, can even completely cover the charge-density wave. Such phase separation does not occur in the related Edwards fermion-boson model.

Introduction

Metal-insulator transitions (MITs) driven by the electron-phonon (EP) coupling have been the focus of solid-state physics studies for decades. The Peierls instability^{1,2} is perhaps the most prominent and fundamental example. Acting in the static (frozen-phonon) limit, it establishes an insulating—charge-density-wave (CDW)—broken-symmetry state, related to a structural distortion, as observed in most one-dimensional (1D) inorganic and organic conductors^{3,4}. Quantum phonon fluctuations, on the other hand, become increasingly important in low dimensions, and counteract any development of long-range order,⁵⁻⁷

While the basic mechanisms promoting or hindering a metal-insulator quantum-phase transition are well known⁸, their detailed understanding within the framework of minimal theoretical models is challenging. Actually there are only a very limited number of microscopic model Hamiltonians for which such an MIT could be rigorously proven. Holstein-like models⁹ provide a paradigm in this respect, both in the spinless and the spinful case^{10,11}. By using involved numerical techniques, such as exact diagonalization and kernel polynomial¹²⁻¹⁵, diagrammatic and quantum Monte Carlo¹⁶⁻¹⁸, or density-matrix renormalization group (DMRG)^{5,19} methods, this type of model could be solved numerically exact in the last years. This concerns the ground-state, spectral, transport and thermodynamic properties in 1D, both for a few particles and for the case of the half-filled band. As a result, in the latter case, the ground-state phase diagram of, e.g., the spinless fermion Holstein model was determined, and it has been shown that an MIT from a (repulsive) Tomonaga-Luttinger-liquid (TLL)^{20,21} to a CDW occurs when the EP coupling is increased at finite phonon frequency²²⁻²⁷.

The original Holstein model considers a spatially localized EP coupling to a dispersionless phonon mode⁹. While extensions regarding the range and kind of the EP coupling and the electron hopping have been discussed for some time²⁸⁻³⁰, the influence of the missing phonon dispersion was recently questioned, but largely only for the few particle (polaron and bipolaron) problem³¹⁻³⁶. Interestingly, it turned out that the phonon dispersion had a profound effect on the transport properties of Holstein and Edwards polarons in 1D. In two dimensions, it has been demonstrated for the spinful Holstein model that the competition between pairing and charge order can be tuned by even a weak bare phonon dispersion⁷. Against this background, it seems necessary to re-examine the influence of phonon dispersion on the TLL-CDW MIT of the spinless fermion Holstein model as well. That is the main purpose of this work. To this end, we extend the model accordingly and determine the ground state and transport properties using unbiased numerical techniques for the 1D infinite half-filled Holstein system. The MIT phase boundary is compared with that of an effective electronic Hamiltonian, derived for weak phonon dispersion in Appendix A. Results for the related Edwards fermion-boson transport model³⁷⁻⁴¹ are presented and discussed in Appendix B.

Model and Methods

The modified Holstein model under consideration is

$$\hat{H} = -t_f \sum_j (\hat{f}_j^\dagger \hat{f}_{j+1} + \text{H.c.}) - g \omega_0 \sum_j \hat{n}_j (\hat{b}_j^\dagger + \hat{b}_j) + \omega_0 \sum_j \hat{b}_j^\dagger \hat{b}_j + t_\omega \sum_j (\hat{b}_j^\dagger \hat{b}_{j+1} + \text{H.c.}), \quad (1)$$

where \hat{f}_j are fermion annihilation operators describing the conduction electrons, \hat{b}_j are boson annihilation operators for the phonons, and $\hat{n}_j = \hat{f}_j^\dagger \hat{f}_j$. Compared with the regular Holstein model, there is an additional nearest-nearest neighbor hopping of the phonons that changes their dispersion to $\omega(k) = \omega_0 + 2t_\omega \cos(k)$. To simplify the notation, we will use $t_f = 1$ as the unit of energy throughout this work.

All our numerical simulations are based on the matrix-product-state (MPS) formalism⁴². For ground-state calculations with finite system sizes, we employ the regular DMRG algorithm⁴³. It is often more efficient, however, to work directly in the thermodynamic limit by using infinite matrix-product states (iMPS). For those simulations we apply the variational uniform MPS algorithm (VUMPS)⁴⁴ to obtain a ground-state approximation, and the time-dependent-variational principle (TDVP)⁴⁵ with bond expansion^{46,47} to carry out time evolutions. Since we consider perturbations that only affect the state in a finite region, the latter amounts to the TDVP method for finite systems with infinite boundary conditions^{48–50}. The maximum bond dimension in our simulations was 400, except for systems with periodic boundary conditions, in which case it was 1600.

The infinite-dimensional local Hilbert spaces of the phonons must be truncated to a finite dimension D_b for the numerical simulations. Depending on the model parameters, one may need a relatively large D_b to accurately represent the low-energy states, particularly in the CDW phase. Several methods have been developed to make MPS simulations more efficient for systems with large local Hilbert spaces⁵¹. Here, we use the pseudo-site approach for the finite-system DMRG calculations⁵². For the VUMPS and TDVP simulations in the TLL phase, we did not utilize any such techniques because we found a relatively small boson dimension $D_b = 8$ to be sufficient.

Results

Phase diagram

To gain insight into the general ground-state phase diagram of the model (1), it is helpful to apply a Lang-Firsov transformation that changes the fermion and boson operators while leaving the fermion density operators \hat{n}_j invariant⁵³. As shown in Appendix A, this transformation reveals an effective electron-electron interaction that is not present in the regular Holstein model with dispersionless phonons. Since the interaction is exponentially decaying with an exponent $\text{arcosh}(\omega_0/|2t_\omega|)$, it suffices to consider only the nearest-neighbor part if the dispersion is small. Applying standard perturbation theory^{10,54} then yields the following purely electronic Hamiltonian that is valid for $t_f/g^2, |t_\omega| \ll \omega_0$:

$$\hat{H}_{\text{eff}} = -\tilde{t}_f \sum_j (\hat{f}_j^\dagger \hat{f}_{j+1} + \text{H.c.}) + \left[\frac{\tilde{t}_f^2}{\omega_0} (4g_1 + 2g_2) + 2t_\omega g^2 \right] \sum_j \hat{n}_j \hat{n}_{j+1} + \frac{\tilde{t}_f^2}{\omega_0} g_1 \sum_j [\hat{f}_{j-1}^\dagger (2\hat{n}_j - 1) \hat{f}_{j+1} + \text{H.c.}], \quad (2)$$

where $\tilde{t}_f = t_f e^{-a^2}$, $g_1 = \sum_{n=1}^{\infty} \frac{a^{2n}}{n!n}$, $g_2 = \sum_{n=1}^{\infty} \sum_{m=1}^{\infty} \frac{a^{2(n+m)}}{n!m!(n+m)}$, and $a = g(1 - t_\omega/\omega_0)$. The main difference compared with the effective model for the regular Holstein model is the additional contribution $\propto t_\omega$ to the interaction term. From Eq. (2) one can draw some qualitative conclusions about the phase diagram. For $t_\omega = 0$, the interaction is always repulsive, and since it decreases slower with g than the effective hopping strength, it causes a transition from a TLL to a CDW as g is increased¹⁰. When t_ω is finite, however, there is an additional term that grows quadratically with g and therefore becomes decisive at strong EP coupling. In particular, it leads to an attractive interaction if $t_\omega < 0$, which indicates the possibility of an attractive TLL, and even phase separation, both of which do not occur in the regular Holstein model. For $t_\omega > 0$, on the other hand, the phonon dispersion should simply move the CDW-TLL transition to lower EP couplings.

Since the effective Hamiltonian (2) has a limited region of validity, it is important to check the above predictions with numerical calculations. Before describing the numerical approach, let us first discuss the resulting phase diagram shown in Fig. 1. For $t_\omega = 0.1$, there is indeed a significant shift of the TLL-CDW transition to lower values of g for all ω_0 . The stronger effect in the adiabatic regime is likely related to the fact that we consider a fixed t_ω , so that the effective interaction becomes longer ranged at small ω_0 . Going to a small negative $t_\omega = -0.0025$, a region with phase separation appears at large g . It is mostly located above the CDW phase, an exception being the anti-adiabatic regime, where the CDW phase disappears and there is a direct transition from a TLL to phase separation. The phase-transition points at strong-coupling can also be estimated by dropping the last term in Eq. (2), which leaves only a t - V Hamiltonian whose phase diagram is known exactly⁵⁵. As demonstrated in Fig. 1(b), the phase-separation boundary obtained this way agrees quite well with that of the full model. Interestingly, the competition between the effective repulsive interaction from perturbation theory and the attractive interaction

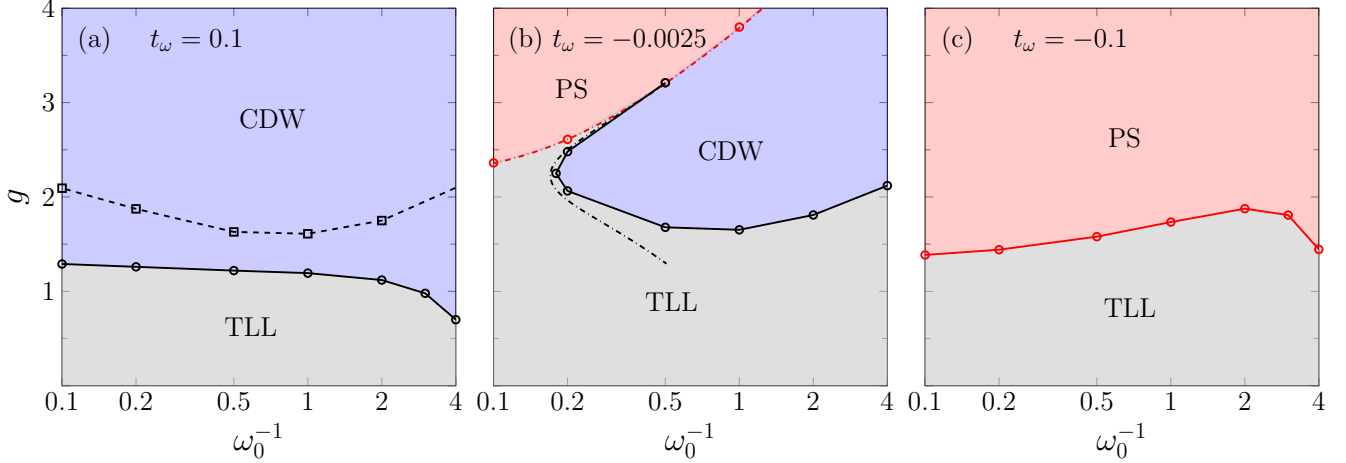


Figure 1. Ground-state phase diagram for different values of the phonon hopping t_ω . Circles mark the numerically calculated phase boundaries, with the solid lines as a guide to the eye. For comparison, the dashed line in (a) shows the TLL-CDW boundary in the dispersionless Holstein model²⁷. The dash-dotted lines in (b) indicate the transitions according to the effective model (2) when neglecting the correlated next-nearest-neighbor hopping.

due to the phonon dispersion causes a reentrant CDW-TLL transition that is visible at $\omega_0 = 5$. When ω_0 is lowered, this second TLL region becomes smaller and effectively disappears. Already at moderate negative hopping $t_\omega = -0.1$, we no longer observe a CDW phase, i.e., the system appears to always be in an attractive TLL or phase-separated state. We would like to point out that, in contrast, the half-filled Edwards model with dispersive bosons neither forms an attractive TLL nor a phase-separated state for negative values of t_ω , see Appendix B.

Within the TLL phase, the system is characterized by the TLL parameter K , which can be used to distinguish between effective repulsive ($K < 1$) and attractive interactions ($K > 1$). Furthermore, $K = 1/2$ signals a transition to the CDW phase, while $K \rightarrow \infty$ indicates the onset of phase separation. There are several ways to numerically determine the TLL parameter K . Here, we use its relation to the linear conductance^{56,57} and the charge structure factor⁵⁸⁻⁶⁰. Figure 2 displays the results for an intermediate phonon energy $\omega_0 = 1$. At weak EP coupling, the TLL parameter is close to the value $K = 1$ of a non-interacting chain of fermions regardless of the phonon parameters. As the EP coupling g increases, however, the effect of the phonon dispersion on K becomes significant. For $t_\omega = 0.1$ and $t_\omega = -0.0025$, K decreases with g up to the TLL-CDW transition where $K = 1/2$, indicating that the TLL for these parameters is repulsive as in the regular Holstein model. In contrast, setting $t_\omega = -0.1$ clearly leads to an attractive TLL with $K > 1$, similar to a sufficiently strong longer-ranged EP coupling⁶¹. The rapid increase of K near $g \approx 1.5$ also suggests that a phase-separation transition is approached. However, while calculating K allows to accurately locate the TLL-CDW transition, it is difficult to prove the occurrence of phase separation in this manner. We therefore also compute the inverse compressibility,

$$\kappa^{-1}(L) = \frac{L}{2} [E_0(L/2 + 1) + E_0(L/2 - 1) - 2E_0(L/2)], \quad (3)$$

where $E_0(N)$ is the ground-state energy for a system with N electrons, and L is the number of sites^{62,63}. For $\omega_0 = 1$ and $t_\omega = -0.1$, $\kappa^{-1} = \lim_{L \rightarrow \infty} \kappa^{-1}(L)$ vanishes around $g \approx 1.74$, which indicates that the system indeed becomes unstable towards phase separation at this point. Furthermore, we found no evidence for electron pairing, i.e., defining $\kappa^{-1}(L)$ in terms of the two-particle gap instead of the single-particle gap as in Eq. (3) does not lead to a smaller κ^{-1} for the parameters considered here. As an alternative to the inverse compressibility, one can also look at the ground-state energy per site ε_0 from an iMPS simulation and extrapolate where it becomes larger than that of a phase-separated state with an empty and a fully occupied subsystem, i.e., where $\Delta\varepsilon = -\frac{1}{2}g^2\omega_0^2/(\omega_0 + 2t_\omega) - \varepsilon_0 = 0$. The transition point obtained this way agrees reasonably well with that from the inverse compressibility, which is why we use this simpler method to determine the remaining phase-separation boundaries.

The TLL-CDW transition can also be determined by locating the breakdown of the CDW state, which is signaled by a closing of the charge gap $\Delta_c = E_0(L/2 + 1) + E_0(L/2 - 1) - 2E_0(L/2)$. Figure 2(c) shows Δ_c in the CDW phase near the phase transitions for model parameters $\omega_0 = 1$ and $t_\omega = -0.0025$. For EP couplings g close to the lower phase boundary, the results are clearly consistent with those for the TLL parameter K , although accurately determining the transition point this way is difficult because of the slow closing of the gap at the Kosterlitz-Thouless transition. Near the second transition, on

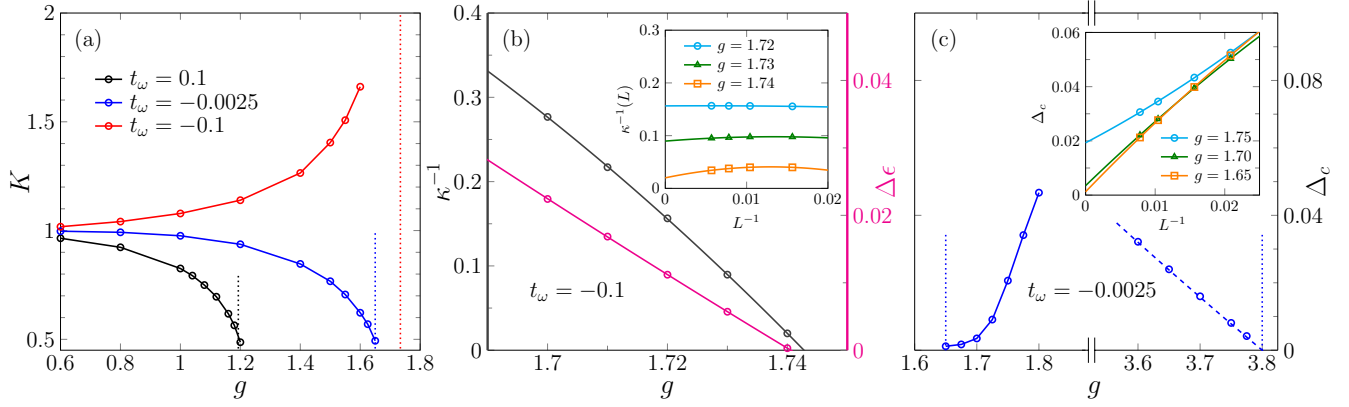


Figure 2. (a) TLL parameter K as a function of the EP coupling g for $\omega_0 = 1$ and different phonon dispersions. Dotted lines mark the locations of phase transitions. (b) Inverse compressibility κ^{-1} and ground-state energy per site $\Delta\epsilon$ relative to a phase-separated state for $\omega_0 = 1$ and $t_\omega = -0.1$. The inset shows the extrapolation from finite-system DMRG calculations of $\kappa^{-1}(L)$ with open boundary conditions. (c) Charge gap in the CDW phase for $\omega_0 = 1$ and $t_\omega = -0.1$. The dashed line shows the charge gap when only the nearest-neighbor-repulsion term is considered in Eq. (2). The calculations were done for finite systems with open boundary conditions and then extrapolated to the thermodynamic limit using a second-order polynomial. For parameters near the TLL-CDW transition the finite-size extrapolation is presented in the inset.

the other hand, the electron motion is almost completely frozen because of the exponential decrease of the effective hopping amplitude \tilde{t}_f with the EP coupling g , so that the charge gap in this region is approximately proportional to the coefficient of the nearest-neighbor interaction in Eq. (2). The closing of the gap coincides with $\Delta\epsilon$ becoming zero, which suggests that only a vanishingly small intermediate TLL phase exists.

Calculation of the Tomonaga-Luttinger parameter K

In the TLL phase the linear conductance at zero temperature is given by $K/(2\pi)^{56}$. Accordingly, one can determine the TLL parameter from the charge-current response to a small voltage V as

$$K = \lim_{t \rightarrow \infty} \lim_{V \rightarrow 0} \frac{2\pi J(t)}{V}. \quad (4)$$

The charge current at time t for an arbitrary bond j is $J_j(t) = -it_f \langle \hat{f}_j^\dagger \hat{f}_{j+1} - \hat{f}_{j+1}^\dagger \hat{f}_j \rangle_t$. Specifically, we apply a constant potential gradient over $L_V = 10$ sites and calculate the average current $J(t)$ in that region. The corresponding perturbation to the Hamiltonian for times $t > 0$ is $\sum_j V_j \hat{n}_j$, with $V_j = \min(\max(-\frac{V}{2} + \frac{jV}{L_V+1}, -\frac{V}{2}), \frac{V}{2})$. Figure 3 shows the obtained current $J(t)$ for parameters near the phase transitions for $\omega_0 = 1$ and $t_\omega = \pm 0.1$. Except for small fluctuations, $J(t)$ saturates with time, which allows to estimate the conductance and thereby K . Only for $t_\omega = 0.1$ and $g = 1.2$, the current $J(t)$ appears to decrease at long times, likely because the system is already slightly in the insulating CDW regime.

Another way to determine the TLL parameter K is the relation⁵⁹

$$K = \lim_{q \rightarrow 0} \frac{2\pi S(q)}{q}, \quad (5)$$

which connects K to the static structure factor $S(q) = \frac{1}{L} \sum_{j\ell} e^{iq(j-\ell)} \langle \hat{n}_j \hat{n}_\ell \rangle$. Although $S(q)$ can be calculated from the iMPS approximation of the ground state, we found that using finite systems with periodic boundary conditions and $K = \lim_{L \rightarrow \infty} LS(2\pi/L)$ leads to a weaker momentum dependence and thus a clearer extrapolation. As demonstrated in Fig. 3, the TLL parameters obtained this way are consistent with the charge current at long times. We also used the approach based on the structure factor for the 3 points in Fig. 1(b) around $\omega_0 = 5$, where we encountered convergence issues in the iMPS method.

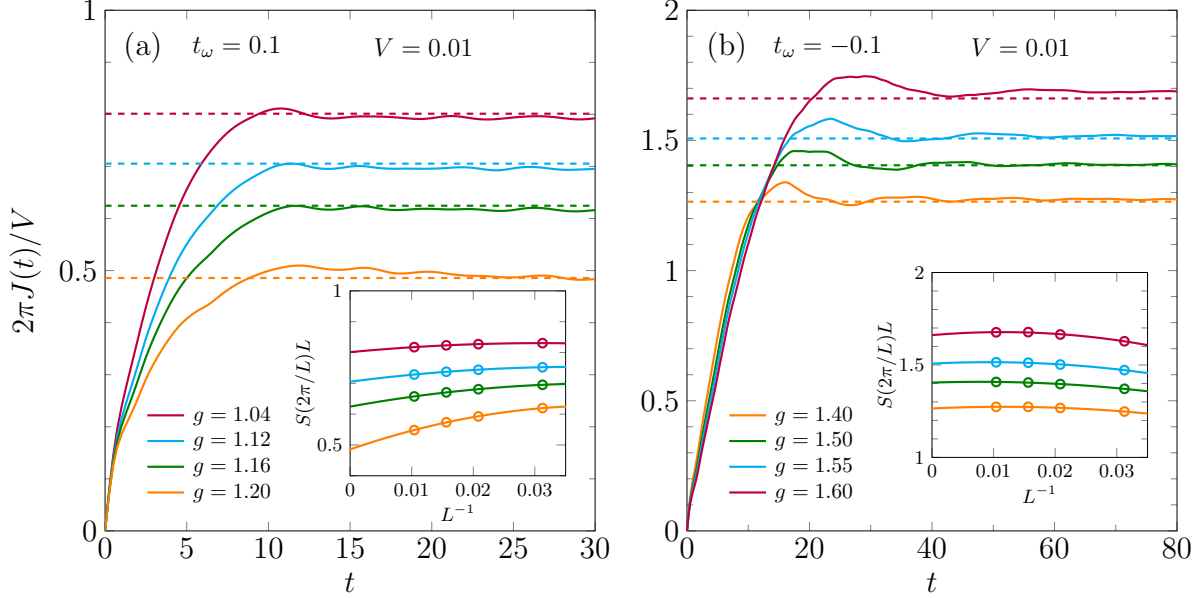


Figure 3. (a), (b) Examples for the calculation of K by means of the charge conductance for $\omega_0 = 1$. The inset of shows an alternative method based on the charge structure factor in finite systems with periodic boundary conditions. In the main panels, the extrapolated values of K are displayed as dashed lines.

Conclusions

We used MPS techniques to numerically investigate the effect of a finite phonon dispersion on the phase diagram of the one-dimensional Holstein model, focusing in particular on the TLL parameter K , which we have extracted from both static and dynamic quantities. In agreement with the derived effective strong-coupling Hamiltonian, our results demonstrate that a downward dispersion increases the tendency to CDW order, while an upward dispersion leads to an effective electron-electron attraction. As the EP coupling is increased, the attractive interaction manifests itself first as a TLL with $K > 1$, and then as phase separation between an empty and a full subsystem. This is markedly different from the phase diagram of the Holstein model without phonon dispersion that consists only of a repulsive TLL and a CDW, but resembles the situation in models with longer-ranged electron-phonon coupling⁶¹. As shown in Appendix B, the corresponding Edwards fermion-boson model also shows no attractive TLL or phase separation.

While we studied the half-filled case in this work, it would also be interesting to investigate the phase diagram at other densities. For example, a downward phonon dispersion and strong EP coupling should lead to phase separation between a CDW and an empty region, since the effective interaction in that case favours a CDW with wave number π . Lastly, it might be worthwhile to consider extensions of the model with other dispersion or more general types of EP coupling. A natural question in this regard is, whether the different effective electron-electron interactions can lead to more exotic phases, such as TLLs with electron pairing, which were observed in purely fermionic chains with specific longer-ranged interactions or pair-hopping terms⁶⁴.

Appendix A: effective electronic Hamiltonian

In the Holstein model with boson dispersion $\omega(k)$, the electron-phonon coupling term can be removed by a Lang-Firsov transformation $\hat{H} \rightarrow e^{\hat{S}} \hat{H} e^{-\hat{S}}$ with $\hat{S} = -\frac{g}{\sqrt{N}} \sum_j \sum_k \omega(k)^{-1} [e^{-ikj} \tilde{b}_k^\dagger - e^{ikj} \tilde{b}_k] \hat{n}_j$ ⁵³. Here, we used the boson operators $\tilde{b}_k = \frac{1}{\sqrt{N}} \sum_j e^{-ikj} \hat{b}_j$ in momentum space. The transformed Hamiltonian is

$$\begin{aligned} \hat{H} = & -t_f e^{-g^2 \sum_{r>0} (F_r - F_{r-1})^2} \sum_j \left[\hat{f}_j^\dagger \hat{f}_{j+1} e^{-g \sum_{r \in \mathbb{Z}} F_r (\hat{b}_{j+r}^\dagger - \hat{b}_{j+1+r}^\dagger)} e^{g \sum_{r \in \mathbb{Z}} F_r (\hat{b}_{j+r} - \hat{b}_{j+1+r})} + \text{H.c.} \right] \\ & + \sum_j \sum_{r=1}^{\infty} V_r \hat{n}_j \hat{n}_{j+r} + \sum_k \omega(k) \tilde{b}_k^\dagger \tilde{b}_k, \end{aligned} \quad (6)$$

where $F_r = \frac{\omega_0}{2\pi} \int_{-\pi}^{\pi} \frac{\cos(kr)}{\omega_0 + 2t_\omega \cos(k)} dk = \frac{1}{\tanh(\alpha)} [-\text{sgn}(t_\omega/\omega_0)]^r e^{-\alpha|r|}$ with $\alpha = \text{arcosh}(\omega_0/|2t_\omega|)$. The most significant effect of the boson dispersion is the electron-electron interaction with coefficients $V_r = 2\omega_0 g^2 F_r$. For small dispersion $|t_\omega| \ll \omega_0$, only the nearest-neighbor term with $V_1 \approx 2t_\omega g^2$ is important, which is repulsive (attractive) for positive (negative) t_ω . As in the model without dispersion^{10,54}, one can apply second-order perturbation theory to Eq. (6) in order to obtain an effective strong-coupling Hamiltonian for $t_f \ll \omega_0 g^2$. The calculation is complicated by the fact that the hopping term for a given electron site involves boson operators over a larger spatial range than in the model without dispersion. For $|t_\omega| \ll \omega_0$, however, we can make the approximations $e^{-g \sum_{r \in \mathbb{Z}} F_r (\hat{b}_{j+r}^\dagger - \hat{b}_{j+1+r}^\dagger)} e^{g \sum_{r \in \mathbb{Z}} F_r (\hat{b}_{j+r} - \hat{b}_{j+1+r})} \approx e^{-g(F_0 - F_1)(\hat{b}_j^\dagger - \hat{b}_{j+1}^\dagger)} e^{g(F_0 - F_1)(\hat{b}_j - \hat{b}_{j+1})}$ and $F_1 - F_0 \approx 1 - t_\omega/\omega_0$, which results in Eq. (2) of the main text.

Appendix B: Edwards fermion-boson model

The Hamiltonian of the 1D modified Edwards model,

$$\hat{H} = -t_{fb} \sum_j \left(\hat{f}_{j+1}^\dagger \hat{f}_j (\hat{b}_j^\dagger + \hat{b}_{j+1}) + \text{H.c.} \right) - \lambda \sum_j (\hat{b}_j^\dagger + \hat{b}_j) + \omega_0 \sum_j \hat{b}_j^\dagger \hat{b}_j + t_\omega \sum_j (\hat{b}_j^\dagger \hat{b}_{j+1} + \text{H.c.}), \quad (7)$$

describes quantum transport in a background medium parametrized by dispersive bosons. Here, a fermion f emits or absorbs a boson b of energy $\omega(k) = \omega_0 + 2t_\omega \cos(k)$ every time it hops between neighboring lattice sites^{35,37}. The bosons can also relax via the λ -term without fermion hopping. When the bosons are dispersionless, a TLL-CDW transition was found for a half-filled band in one dimension³⁹⁻⁴¹. In the Edwards model, the insulating phase is realized for a stiff background, i.e., at small λ and large ω_0 . The question now is how the dispersion of the bosons influences the position of the MIT phase boundary and in particular whether an attractive TLL or phase separation also occurs in the Edwards model when $t_\omega < 0$. To address this, we use the same numerical approach as for the Holstein model and determine the TLL parameter K by calculating the charge current due to a small voltage $V = 0.01$, using t_{fb} as the unit of energy. Figure 4(a) displays the obtained K values for $\omega_0 = 2$ and $t_\omega = \pm 0.1$. The TLL-CDW transition, where $K = 1/2$, is significantly shifted by the added boson dispersion. Obviously, the CDW region gets—by and large—bigger for positive t_ω (cf. data for $t_\omega = 0.1$) while it becomes smaller for negative t_ω (see results for -0.1). As shown in Fig. 4(b), this trend also applies to other boson energies ω_0 . The only exception is the region of small ω_0 and λ , where both the downward and upward boson dispersions reduce the CDW region. In fact, the sign of the boson hopping does not affect the phase at $\lambda = 0$, since there it can be changed by a gauge transformation of the fermions and bosons $(\hat{f}_j, \hat{b}_j) \rightarrow (i^{j^2} \hat{f}_j, i(-1)^{j+1} \hat{b}_j)$. The most important difference to the spinless fermion Holstein model, however, is the absence of phase separation for $t_\omega = -0.1$.

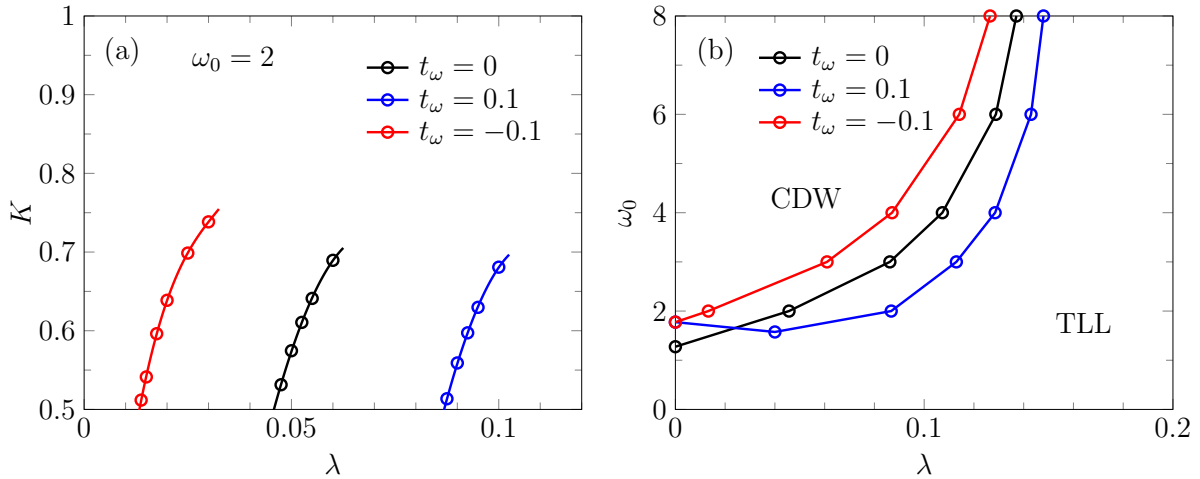


Figure 4. (a) TLL parameter in the Edwards model with dispersive bosons and (b) the corresponding ground-state phase diagram.

Data availability

The data that support the findings of this study are available from the corresponding author upon reasonable request.

References

1. Peierls, R. *Quantum theory of solids* (Oxford University Press, Oxford, 1955).
2. Fröhlich, H. *Adv. Phys.* **3**, 325 (1954).
3. Grüner, G. *Density Waves in Solids* (Addison Wesley, Reading, MA, 1994).
4. Pouget, J.-P. *C. R. Phys.* **17**, 332 (2016).
5. Jeckelmann, E., Zhang, C. & White, S. R. *Phys. Rev. B* **60**, 7950 (1999).
6. Hohenadler, M. & Fehske, H. *Eur. Phys. J. B* **91**, 204 (2018).
7. Costa, N. C., Blommel, T., Chiu, W.-T., Batrouni, G. & Scalettar, R. T. *Phys. Rev. Lett.* **120**, 187003 (2018).
8. Mott, N. F. *Metal-Insulator Transitions* (Taylor & Francis, London, 1990).
9. Holstein, T. *Ann. Phys. (N.Y.)* **8**, 325 (1959).
10. Hirsch, J. E. & Fradkin, E. *Phys. Rev. B* **27**, 4302 (1983).
11. Zhao, S., Han, Z., Kivelson, S. A. & Esterlis, I. *Phys. Rev. B* **107**, 075142 (2023).
12. Weiße, A., Fehske, H., Wellein, G. & Bishop, A. R. *Phys. Rev. B* **62**, R747 (2000).
13. Fehske, H. & Trugman, S. A. In Alexandrov, A. S. (ed.) *Polarons in Advanced Materials*, vol. 103 of *Springer Series in Material Sciences*, 393–461 (Canopus/Springer Publishing, Dordrecht, 2007).
14. Sykora, S., Hübsch, A., Becker, K. W., Wellein, G. & Fehske, H. *Phys. Rev. B* **71**, 045112 (2005).
15. Weiße, A., Wellein, G., Alvermann, A. & Fehske, H. *Rev. Mod. Phys.* **78**, 275 (2006).
16. Mishchenko, A. S., Nagaosa, N. & Prokof'ev, N. *Phys. Rev. Lett.* **113**, 166402 (2014).
17. Hohenadler, M., Fehske, H. & Assaad, F. F. *Phys. Rev. B* **83**, 115105 (2011).
18. Weber, M., Assaad, F. F. & Hohenadler, M. *Phys. Rev. B* **94**, 245138 (2016).
19. Jeckelmann, E. & Fehske, H. *Rivista del Nuovo Cimento* **30**, 259 (2007).
20. Tomonaga, S. *Prog. Theor. Phys.* **5**, 544 (1950).
21. Luttinger, J. M. *J. Math. Phys.* **4**, 1154 (1963).
22. Zheng, H., Feinberg, D. & Avignon, M. *Phys. Rev. B* **39**, 9405 (1989).
23. Weiße, A. & Fehske, H. *Phys. Rev. B* **58**, 13526 (1998).
24. McKenzie, R. H., Hamer, C. J. & Murray, D. W. *Phys. Rev. B* **53**, 9676 (1996).
25. Bursill, R. J., McKenzie, R. H. & Hamer, C. J. *Phys. Rev. Lett.* **80**, 5607 (1998).
26. Hohenadler, M., Wellein, G., Bishop, A. R., Alvermann, A. & Fehske, H. *Phys. Rev. B* **73**, 245120 (2006).
27. Ejima, S. & Fehske, H. *Eur. Lett.* **87**, 27001 (2009).
28. Alexandrov, A. S. & Kornilovitch, P. E. *Phys. Rev. Lett.* **82**, 807 (1999).
29. Fehske, H., Loos, J. & Wellein, G. *Phys. Rev. B* **61**, 8016 (2000).
30. Hohenadler, M. *Phys. Rev. Lett.* **117**, 206404 (2016).
31. Marchand, D. J. J. & Berciu, M. *Phys. Rev. B* **88**, 060301 (2013).
32. Bonča, J. & Trugman, S. A. *Phys. Rev. B* **103**, 054304 (2021).
33. Bonča, J. & Trugman, S. A. *Phys. Rev. B* **106**, 174303 (2022).
34. Jansen, D., Bonča, J. & Heidrich-Meisner, F. *Phys. Rev. B* **106**, 155129 (2022).
35. Chakraborty, M. & Fehske, H. *Phys. Rev. B* **109**, 085125 (2024).
36. Kovač, K. & Bonča, J. *Phys. Rev. B* **109**, 064304 (2024).
37. Edwards, D. M. *Phys. B* **378-380**, 133 (2006).
38. Alvermann, A., Edwards, D. M. & Fehske, H. *Phys. Rev. Lett.* **98**, 056602 (2007).
39. Wellein, G., Fehske, H., Alvermann, A. & Edwards, D. M. *Phys. Rev. Lett.* **101**, 136402 (2008).
40. Ejima, S., Hager, G. & Fehske, H. *Phys. Rev. Lett.* **102**, 106404 (2009).

41. Lange, F., Wellein, G. & Fehske, H. *Phys. Rev. Res.* **6**, L022007 (2024).
42. Schollwöck, U. *Ann. Phys.* **326**, 96–192 (2011).
43. White, S. R. *Phys. Rev. Lett.* **69**, 2863 (1992).
44. Zauner-Stauber, V., Vanderstraeten, L., Fishman, M. T., Verstraete, F. & Haegeman, J. *Phys. Rev. B* **97**, 045145 (2018).
45. Haegeman, J., Lubich, C., Oseledets, I., Vandereycken, B. & Verstraete, F. *Phys. Rev. B* **94**, 165116 (2016).
46. Gleis, A., Li, J.-W. & von Delft, J. *Phys. Rev. Lett.* **130**, 246402 (2023).
47. Li, J.-W., Gleis, A. & von Delft, J. (2022). arXiv:2208.10972.
48. Phien, H. N., Vidal, G. & McCulloch, I. P. *Phys. Rev. B* **86**, 245107 (2012).
49. Milsted, A., Haegeman, J., Osborne, T. J. & Verstraete, F. *Phys. Rev. B* **88**, 155116 (2013).
50. Zauner, V., Ganahl, M., Evertz, H. G. & Nishino, T. *J. Phys.: Condens. Matter* **27**, 425602 (2015).
51. Stolpp, J. *et al. Comput. Phys. Commun.* **269**, 108106 (2021).
52. Jeckelmann, E. & White, S. R. *Phys. Rev. B* **57**, 6376 (1998).
53. Lang, I. G. & Firsov, Y. A. *Zh. Eksp. Teor. Fiz.* **43**, 1843 (1962).
54. Datta, S., Das, A. & Yarlagadda, S. *PRB* **71**, 235118 (2005).
55. Giamarchi, T. *Quantum Physics in One Dimension* (Clarendon Press, Oxford, 2003).
56. Kane, C. L. & Fisher, M. P. A. *Phys. Rev. B* **46**, 15233 (1992).
57. Kang, Y.-T., Lo, C.-Y., Oshikawa, M., Kao, Y.-J. & Chen, P. *Phys. Rev. B* **104**, 235142 (2021).
58. Giamarchi, T. & Schulz, H. J. *Phys. Rev. B* **39**, 4620 (1989).
59. Ejima, S., Gebhard, F. & Nishimoto, S. *Eur. Lett.* **70**, 492 (2005).
60. Karrasch, C. & Moore, J. E. *Phys. Rev. B* **86**, 155156 (2012).
61. Hohenadler, M., Assaad, F. F. & Fehske, H. *Phys. Rev. Lett.* **109**, 116407 (2012).
62. Ogata, M., Luchini, M. U., Sorella, S. & Assaad, F. F. *Phys. Rev. Lett.* **66**, 2388 (1991).
63. Ejima, S., Sykora, S., Becker, K. W. & Fehske, H. *Phys. Rev. B* **86**, 155149 (2012).
64. Gotta, L., Mazza, L., Simon, P. & Roux, G. *Phys. Rev. Lett.* **126**, 206805 (2021).
65. Fishman, M., White, S. R. & Stoudenmire, E. M. *SciPost Phys. Codebases* 4 (2022).
66. Fishman, M., White, S. R. & Stoudenmire, E. M. *SciPost Phys. Codebases* 4–r0.3 (2022).

Acknowledgements

The authors acknowledge the scientific support and HPC resources provided by the Erlangen National High Performance Computing Center (NHR@FAU) of the Friedrich-Alexander-Universität Erlangen-Nürnberg (FAU). The hardware is funded by the German Research Foundation (DFG). MPS simulations were performed using the ITensor library^{65,66}.

Author contributions statement

F.L. and H.F. contributed equally to this work.

Additional information

Competing interests The authors declare no competing financial interests.